BEHAVIOUR OF HIGH-STRENGTH MIX REINFORCED CONCRETE BEAMS

S.M. SERAJ (Dhaka), M.D. KOTSOVOS (Athens),
M.N. PAVLOVIĆ (London)

The work presently described forms part of a comprehensive research programme which aims at introducing a unified design approach to the design of reinforced and prestressed concrete structures, made from both normal- and high-strength concrete. Current methods for the design of reinforced concrete members *on the basis of ultimate-strength philosophy* are based on concepts which do not comply with the fundamental behaviour of concrete at the material level. In this paper, it is shown through experimental evidence that the physical model based on the concept of compressive-force path, which seems capable of explaining *rationally* the behaviour of normal strength concrete members, can also be used in the design of reinforced concrete members made from high-strength mixes. Furthermore, it is demonstrated that, for a high-strength concrete element to attain its flexural capacity, it does not have to behave like a 'truss'. On the contrary, design based on the 'truss' model may become inefficient and expensive. A limited numerical parametric study and supporting evidence from past laboratory experimentation have been included in the paper which show that the role of flange reinforcement in a high-strength concrete member is less pronounced than in its normal-strength counterpart. This finding has been explained in the light of varying degrees of triaxiality that prevail in normal- and high-strength concrete elements.

NOTATION

A_s area of longitudinal tension reinforcement which continues for a distance at least equal to d beyond section being considered,
A_{sv} area of transverse reinforcement,
b_1 effective width (see Fig. A1),
C compressive force in concrete,
CFP compressive-force path,
d effective depth (mm),
f_{cu} uniaxial compressive cube strength of concrete,
f_{cyl} uniaxial cylinder strength,
FE finite element,
f_y characteristic (yield) strength of tension steel (N/mm^2),

f_{yv} yield stress of stirrup material,
HSC high-strength concrete,
M_c moment corresponding to failure load (Nmm),
M_f flexural capacity (Nmm),
NSC normal-strength concrete,
RC reinforced concrete,
s distance from support of cross-section at which M_c is calculated (mm) (equal to shear span for point loading, and 2d for uniformly distributed loading in RC members),
T tensile force in longitudinal steel,
T_{sv} transverse tensile force,
V_a applied shear force,
V_c tensile force resisted by concrete alone in region where CFP changes direction,
V_s shear force carried by shear reinforcement,
X depth of neutral axis,
x' depth of neutral axis considering triaxial conditions,
X_g centroidal distance of uncracked concrete from compression face,
z lever-arm distance,
Δz increase in lever arm,
ϕ bar size,
θ crack angle,
ρ_w tension steel ratio (A_s/bd),
σ'_c nominal triaxial compressive stress,
σ_c 0.8 f_{cyl}, 0.64–0.67 f_{cu},
σ_{conf} confining pressure required for σ_c to increase to σ'_c,
σ_t transverse tensile stress,
3-D three-dimensional.

1. INTRODUCTION

Current CODES [1–4] are generally based on the view that the major contribution to shear resistance in beams is provided by the region below the neutral axis, a prerequisite for the widely-accepted notion that the shear capacity of an RC beam is to be defined as the maximum shear force that can be sustained by a critical cross-section, with shear reinforcement being provided in order to carry that portion of the shear force that cannot be sustained by concrete alone. The amount of reinforcement required for this purpose is assessed by using one of a number of available methods that are invariably developed on the basis of the 'truss-analogy' concept [5, 6], the latter stipulating that an RC beam with shear reinforcement behaves as a 'truss' once inclined cracking occurs. Recent

test results [7–9], however, clearly raise doubts over the validity of the concepts underlying Code provisions, as well as over the effectiveness (in terms of both safety and economy) of the ensuing design solutions.

Although new concepts (e.g. compression field theory [10], modified compression field theory [11], and strut-and-tie model [12] have recently evolved in the general field of structural concrete design — with claims of far-reaching potential — most of these deviate very little from the basis on which present-day design is founded; and, thus, they carry implicit assumptions which, in many cases, are incompatible with the fundamental properties of concrete. The concept of 'compressive force path' (*CFP*) [13], on the other hand, departs radically from the established design concepts, and seems to give an adequate and rational explanation of the behaviour of structural concrete. So far, however, the design model stemming from this concept has been applied to *RC* beams [7] and shear walls [14] made exclusively from normal-strength concrete (*NSC*).

These days, modern technology allows the production of very high-strength workable concrete mixes. As a result, the design of structural members made from high-strength concrete (*HSC*) is also gaining momentum. Presently, empirical formulae derived originally for *NSC* beams are usually also used for the design of such members. It is apparent, therefore, that design procedures based on a fundamental understanding of *HSC* beam behaviour at the ultimate limit state would be preferable to the current approach of mere extrapolation. Only a very limited amount of research has, so far, been conducted in the field of *HSC* structural elements. Unfortunately, the researchers [15–18] merely tested a few beams made from *HSC* and tried either to develop new equations on the basis of this limited number of tests, or attempted to criticize the existing Code equations in the light of their test results. As such, any criticism has been limited to the accuracy of the Code equations themselves, whereas the concepts that form the basis of such Codes remain untouched — very much in line with the traditional thinking and research in the field of concrete structures. It is interesting to note that, while some researchers [15, 16] concluded that for *HSC* beams without web steel the ACI Code may overestimate the shear strength by 10 to 30%, others [17, 18] found ACI Code equations conservative when applied to *HSC* members. (It may be interesting to note that, apart from proposing a new equation, MPHONDE and FRANTZ [17, 18] opined that aggregate interlock — considered, by current thinking, to provide a major contribution to shear strength — does not have much influence on the ultimate strength of structures made from *HSC*; the *CFP* concept, on the other hand, completely ignores any contribution of aggregate interlock irrespective of concrete strength.)

In view of the above, it is the purpose of the present paper to contribute to a better understanding of the structural behaviour of *RC* members made from *HSC* mixes. More particularly, the paper aims at:

a) presenting a critical insight on the present-day design procedures for *RC* members;

b) demonstrating, through physical tests, that the applicability of the *CFP* model as a realistic design concept for concrete structures also extends to *HSC* members;

c) providing experimental evidence to show the inadequacy of Code provisions in the design of *HSC* beams;

d) comparing the behaviour of *HSC* members with their *NSC* counterparts;

e) probing the role of flange reinforcement in a *HSC* member by means of analytical modelling;

f) assisting in a unification of design concepts, based on the true understanding of concrete at the material level.

Although the general principles embodied in the present investigation are applicable to any cross-sectional shape of beam, the study concentrates on the behaviour of *T*-beams. One reason for this is the widespread use of in-situ slab and girder construction which is often designed on the basis of separate plate and beam actions even though the monolithic nature of the structure means that, in reality, a *T*-section design would be more realistic. Furthermore, by designing such beams (i.e. the 'web') as rectangular sections, the critical load-transfer mechanism occurring in the slab (i.e. the 'flange') is missed altogether.

2. DESIGN METHOD

This section presents a brief description of the basic concepts behind the *BS* 8110 provisions and the proposed *CFP* methodology respectively, as *RC* members designed to both these philosophies are to be investigated.

BS 8110 uses the 'truss' model of Fig. 1a, after recognizing the contribution of concrete, in the design of an *RC* member. The traditional truss-analogy is based on the assuptions that *RC* beams with inclined cracking can be modelled by a pin-jointed 'truss'. The top and bottom chords of the 'truss' are the concrete compression zone and longitudinal tension reinforcement respectively. The diagonal struts and vertical ties consist of the beam web and reinforcement (see Fig. 1a). In the most common form, the crack angle, θ, is assumed to be 45°. *BS* 8110 assumes that the total applied shear force is partly carried by concrete (V_c) while the remainder is carried by shear reinforcement (V_s). The term V_c is considered to represent the shear resistance of three separate components, namely a) shear resistance of the uncracked concrete within the compressive zone, b) shear resistance due to aggregate interlock, and c) shear resistance due to dowel action of the longitudinal reinforcement. It is usually assumed [19] that b) and c) provide up to 75% of V_c. Moreover, in a flanged member (say, *T*-beam), the value of V_c is

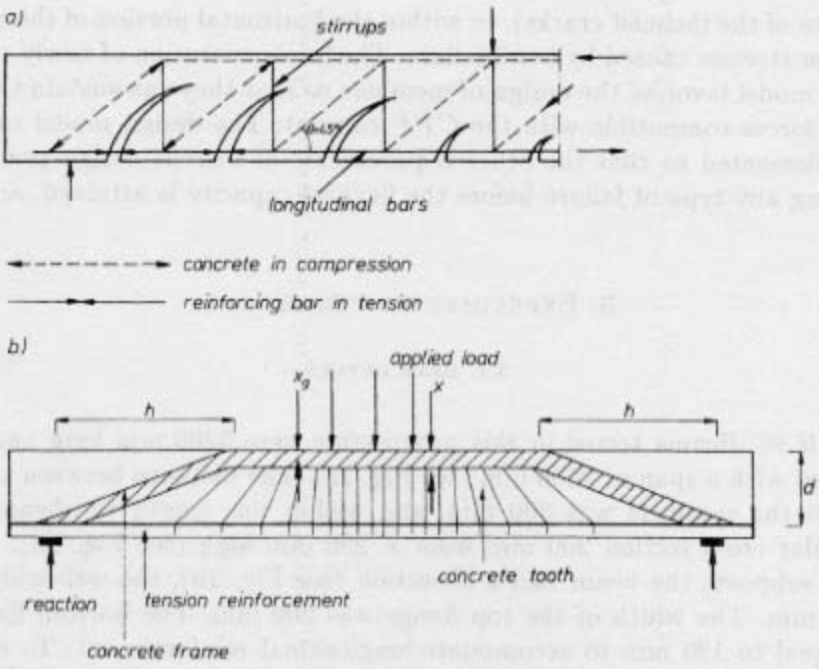

RC BEAM:
$h = 2d$, for point load with $a_v/d > 2$,
$h = a_v$, for point load with $a_v/d \leq 2$,
$h = 2d$, for udl with $L/d > 8$,
$h = L/4$, for *udl* with $L/d \leq 8$,

where,
a_v = shear span in case of point load,
d = effective depth of member,
h = horizontal projection of inclined portion of CFP,
L = length of member,
udl = uniformly distributed load.

FIG. 1. Modelling of a beam. (*a*) — Classical truss-analogy and (*b*) — compressive-force path concept.

Rys. 1. Modelowanie belki żelbetowej. (*a*) — Klasyczny model kratownicowy, (*b*) — model oparty na drodze przebiegu siły ściskającej

considered to be directly proportional to the web-width, signifying that the Code provisions underestimate the contribution of the flange. To avoid failure of the 'truss' model due to web crushing, *BS* 8110 also specifies a maximum limit of allowable shear stress.

On the other hand, the *CFP* concept stipulates that the strength of an *RC* member is associated with the strength of concrete in the region of the path along which the compressive forces are transmitted. Figure 1b shows the 'frame-like' physical model developed for the design of *RC* beams [7]. The path of the compressive force may be visualized as a 'flow' of compressive stresses with varying sections perpendicular to the path direction and with the compressive force representing the stress resultant at each section. Failure may occur either in the region where the *CFP* changes direction (with the setting up of large tensile stresses in

the region of the inclined cracks), or within the horizontal portion of the path due to tension stresses caused by bond failure. The implementation of newly-proposed physical model involves the design of members so that they can sustain the actual internal forces compatible with the *CFP* concept. The design model can, then, be complemented so that the other requirements of current design practice, for preventing any type of failure before the flexural capacity is attained, are met.

3. EXPERIMENTAL PROGRAMME

3.1. BEAM DETAILS

All the *HSC* Beams tested in this programme were 3200 mm long and simply supported with a span of 2600 mm (see Fig. 2a). The distance between the beam ends and the supports was 300 mm, and within this length the beams had a rectangular cross section 200 mm wide × 290 mm high (see Fig. 2b). Between the two supports the beam had a *T*-section (see Fig. 2b), the web width being only 50 mm. The width of the top flange was 200 mm. The bottom flange was made equal to 120 mm to accomodate longitudinal reinforcement. To eliminate the possibility of anchorage failure, the main longitudinal steel bars were extended to about 280 mm beyond the support and screwed onto 100 mm × 100 mm × 10 mm steel end plates, as indicated in Fig. 2c.

The beams were under-reinforced with two 20 mm diameter high-yield deformed bars. At the top of the flange of the beam, 4 mm diameter mild-steel bars were placed in the longitudinal direction, their purpose being to form part of a proper reinforcement cage rather than to contribute to flexural capacity. To prevent possible splitting along the interface between the longitudinal steel bars and concrete (due to large anchoring forces near failure), the end zones of the beams were reinforced with 6 mm diameter high-yield steel links (see also Fig. 2c). Transverse reinforcement was provided by either 6 mm diameter high-yield steel links (see also Fig. 2c). Transverse reinforcement was provided by either 6 mm diameter high-yield deformed bars or 1.5 mm diameter plane wire. Table 1 summarizes the strength characteristics of different bars employed in this programme.

The design cube strength for the *HSC* beams was 80 MPa, and the same concrete mix proportions were used for the casting of all the specimens. The required strength was achieved using normal techniques with high-quality ingredients, a low water/cement ratio, and the addition of chemical admixture (superplasticizer — this allowed the concrete to be produced with a low water/cement ratio but with high slumps (80–90 mm)). The reduction in the water requirements increased the strength without impairing workability. Table 2 gives details of the mix proportions used.

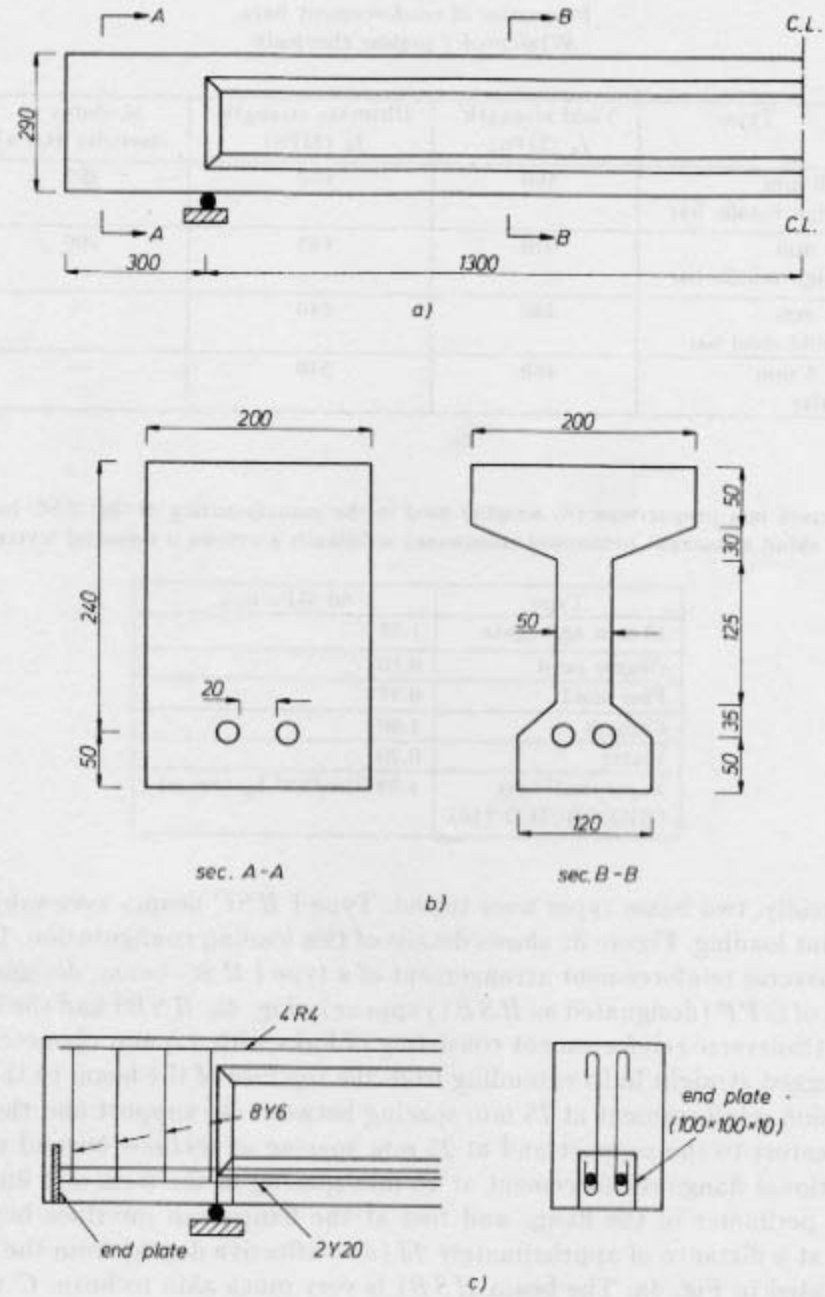

FIG. 2. (*a*) and (*b*) — cross-sectional characteristics and (*c*) — reinforcement details of end zones of *HSC* beams (all dimensions and bar sizes in mm).

Rys. 2. Belki z betonu o dużej wytrzymałości; (*a*) i (*b*) — charakterystyki przekroju, (*c*) — szczegóły zbrojenia stref przypodporowych

Table 1

Properties of reinforcement bars.
Właściwości prętów zbrojenia

Type	Yield strength f_y (MPa)	Ultimate strength f_u (MPa)	Modulus of elasticity (GPa)
20 mm high tensile bar	500	650	205
6 mm high tensile bar	570	665	200
4 mm mild steel bar	460	540	—
1.5 mm wire	460	510	—

Table 2

Concrete mix proportions (by weight) used in the manufacturing of the *HSC* beams.
Wagowy skład mieszanki betonowej stosowanej w belkach z betonu o wysokiej wytrzymałości

Type	80 MPa mix
10 mm aggregate	1.58
Coarse sand	0.86
Fine sand	0.37
Cement	1.00
Water	0.29
Superplasticizer (RHEOBUILD 716)	2.09 litre/100 kg cement

Broadly, two beam types were tested. Type I *HSC* beams were subjected to four-point loading. Figure 3a shows details of this loading configuration. Details of the transverse reinforcement arrangement of a type I *HSC* beam, designed to the concept of *CFP* (designated as *HSB*1) appear in Fig. 4a. *HSB*1 had the following type of transverse reinforcement consisting of links with 1.5 mm diameter: a) two single-legged straight links extending from the top face of the beam to the level of the tension reinforcement at 75 mm spacing between the support and the loading point nearest to the support and at 25 mm spacing at sections beyond that, and b) additional flange reinforcement at 25 mm spacing in the form of a link following the perimeter of the flange and tied at the flange-web interface beyond the section at a distance of approximately $2d$ (d — effective depth) from the support, as indicated in Fig. 4a. The beam *HSB*1 is very much akin to beam *C* tested by KOTSOVOS and LEFAS [7] which was also designed in compliance with the *CFP* concept. Thus, although the properties of the transverse reinforcement of *HSB*1 were slightly different from beam *C*, its arrangement was similar to the latter.

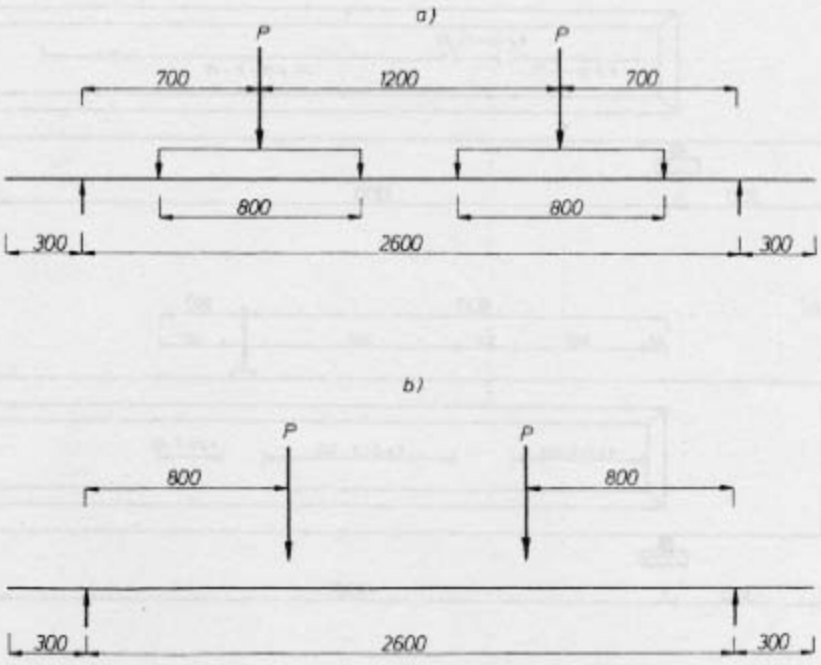

FIG. 3. Loading configurations used for *HSC* beam tests; (*a*) — type I (*HSB*1 and *HSB*4); (*b*) — type II (*HSB*2, *HSB*3 and *HSB*5), (all dimensions in mm).

Rys. 3. Schematy obciążeń w badaniach belek z betonu o dużej wytrzymałości; (*a*) — typ I (*HSB*1 i *HSB*4), (*b*) — typ II (*HSB*2, *HSB*3 i *HSB*5), (wszystkie wymiary w mm)

The type II *HSC* beams were subjected to two-point loading. The adopted loading configuration is shown in Fig. 3b. Experimental results of two type II *HSC* beams, one designed to the concept of *CFP* (designated as *HSB*2) and the other designed to *BS* 8110 (designated as *HSB*3), are to be presented here. Figures 4b and 4c show the details of the transverse reinforcement arrangement of beams *HSB*2 and *HSB*3, respectively. Beam *HSB*2 had two types of transverse reinforcement. Type 1 comprised two single-legged straight links extending from the top face of the beam to the level of the tension reinforcement. Type 2 transverse reinforcement consisted of type 1 reinforcement plus additional links around the perimeter of the top flange. Type 2 transverse reinforcement was placed within the portion of the shear span between the loading point and the section lying at a distance about 2*d* from the support. The remaining portion of the shear span was provided with type 1 links. All the links were made from 6 mm diameter high-yield steel and were placed at 120 mm centre to centre. It is to be noted here that, in the transverse reinforcement details of Fig. 4, $8\phi 1.5-1-25$ means that 1.5 mm diameter type 1 links are placed 25 mm centre to centre; the total no of legs of such vertical links being 8. This notation applies throughout the figure.

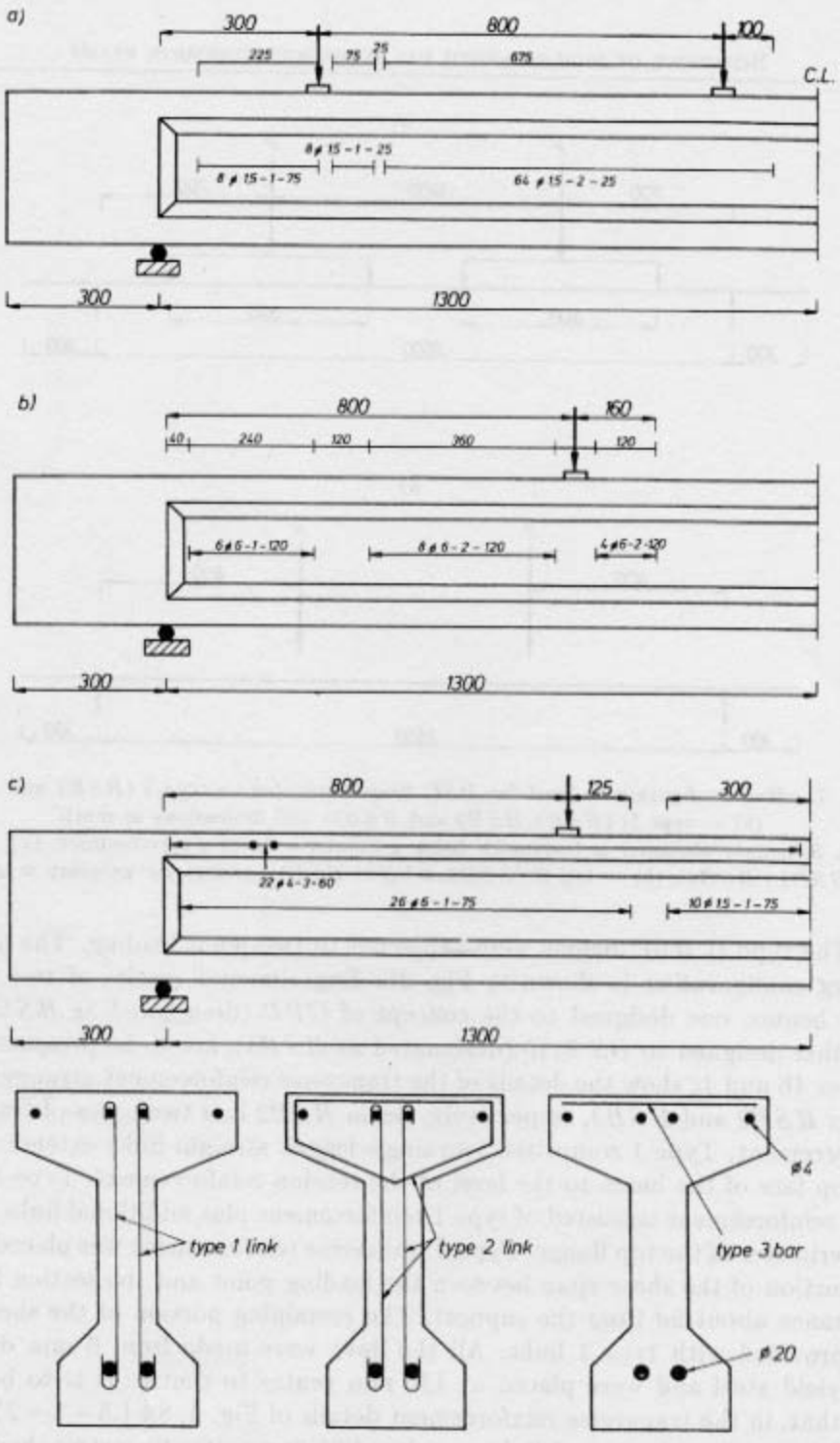

Note: Transverse reinforcement details have been presented in the form $k\phi 1 - m - n$, where, k = total number of legs of links; number of bars, l = diameter of link or bar, m = type of link or bar, n = link or bar spacing.

FIG. 4. Transverse reinforcement details of (a) — $HSB1$, (b) — $HSB2$ and (c) — $HSB3$ (all dimensions and bar sizes in mm).

Rys. 4. Szczegóły zbrojenia w przekrojach poprzecznych belek (a) — $HSB1$, (b) — $HSB2$ i (c) — $HSB3$ (wszystkie wymiary w mm)

In beam *HSB*3, type 1 links made from 6 mm high-yield steel were placed throughout the shear span. In the flexural span, nominal type 1 links made from 1.5 mm diameter steel were also placed. All these links were spaced 75 mm centre to centre. In this beam, a third variety of reinforcement (designated as type 3), comprising a straight 4 mm diameter mild steel bar was used. Type 3 bars were placed at the top of the top flange at 60 mm spacing.

Table 3

Concrete strength characteristics of the various *HSC* beams tested.
Dane o wytrzymałosci betonu w różnych typach badanych belek z betonu o dużej wytrzymałości

Beam	Time of testing, days	Cube strength, MPa		Cylinder strength, MPa
		28 days	Testing day	Testing day
*HSB*1	121	81.2	84.4	69.5
*HSB*2	86	80.7	86.5	70.2
*HSB*3	82	81.0	83.6	69.1

The concrete strength characteristics of these beams are given in Table 3. In the preliminary design calculation of the beams, 80% of the cube strength was assumed as the equivalent uniaxial cylinder compressive strength of concrete. The actual cylinder strength was established on the day of testing.

3.2. TESTING

A testing rig (consisting mainly of four steel uprights, one steel box girder, four concrete reaction blocks and three hydraulic jacks — see Fig. 5) was designed for the purpose of loading beams of various sizes under different loading arrangements to failure. The two-point loading was applied using two 20 ton Amsler static jacks hydraulically connected in series to the testing machine. The load from the jacks was applied to the beam through a 50 mm × 50 mm × 200 mm steel block with one of the two smaller dimensions along the length of the beam. The four-point loading was applied using the same pair of jacks connected in series and two spreader beams. A Bell and Howell pressure transducer in the hydraulic supply line to the Amsler machine ram provided the means of accurate measurement of the applied load.

Deformations were measured by a number of linear voltage differential transducers (LVDTs). The midspan deflection, the 0.30 span deflection and the out-of-plane displacements were recorded. There were 2 LVDTs at the midspan, 2 on the sides to measure out-of-plane displacement and 1 LVDT at each of the 0.30 span locations from the support of the beam. The steel strain in the stirrups of one of the *HSC* beams (*HSB*3 — designed to *BS*8110) tested was measured to calculate the level to which those stirrups were stressed and thus find the stirrup

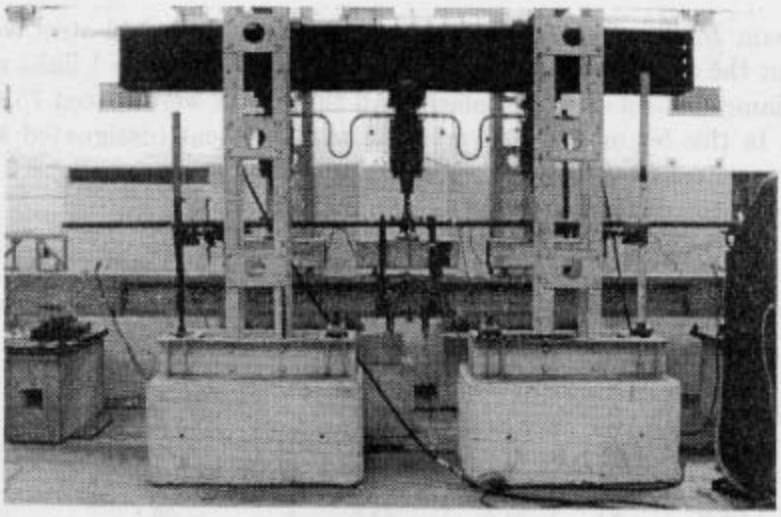

FIG. 5. Test rig.
Rys. 5. Stanowisko do badań

effectiveness in a high-strength concrete beam. At each load increment, the load was maintained constant for about 3 minutes in order to monitor the load and deformation response of the beam, mark the cracks (if any), and take photographs of the member's crack patterns. The measured values of load, displacement, and strain were recorded by a computer-logger capable of measuring to a sensitivity of ±0.1 N, ±0.0001 mm, and ±12 micro-strains, respectively with a speed of about 10 channels per second.

Details of the loading, instrumentation, testing procedure, loading sequence, and the validation of the testing set-up are available elsewhere [9].

4. DISCUSSION OF RESULTS

4.1. LOAD-CARRYING CAPACITY

The provision of transverse reinforcement as dictated by the concept of *CFP* [7, 9], was adopted in the design of type I *HSC* beam *HSB*1. The design details of *HSB*1 have been described in Appendix A. This transverse reinforcement is deemed sufficient for an *RC* beam to attain its flexural capacity. The load-carrying capacity of beam *HSB*1, as calculated using the proposed method, together with the strength value obtained from the actual test, as well as the values predicted by *BS* 8110 and *ACI* 318–89 are given in Table 4. The factor of safety was considered to be equal to 1.0. It should be noted that the Code-predicted failure loads (similar for both *BS* 8110 and *ACI* 318–89) are a direct consequence of the conditions

Table 4

Predicted and actual failure loads of the various *HSC* beams tested.
Obliczone i faktyczne obciążenia niszczące dla różnych badanych belek z betonu o wysokiej wytrzymałości

Beam	Load type	Predicted failure load, kN			Experimental failure load, kN	Predicted/Measured load		
		BS 8110	*ACI* 318	*CFP*		*BS* 8110 / Expt.	*ACI* 318 / Expt.	*CFP* / Expt.
*HSB*1	Four-point	46.74	41.24	224.68	225.0+ 2.0* = 227.0	0.21	0.18	0.99
*HSB*2	Two-point	140	121.52	196.6	200	0.70	0.61	0.98
*HSB*3	Two-point	150	159.43	196.6	201	0.75	0.79	0.98

* Weight of steel spreader beams.

imposed by it (in compliance with the truss-analogy concept), one of which is the notion of the shear capacity of the 'critical' section. It is to be noted that the short segment subjected to the greatest shear force in this beam demands a very high amount of transverse reinforcement according to current design thinking. On the other hand, this portion of the beam falls within the inclined leg of the concrete frame of the *CFP* and hence nominal transverse reinforcement is deemed sufficient. Consequently, the Codes predict a very low failure load as current Codes overestimate the significance of stirrups within this span. It becomes evident from Table 4 that the present Code provisions are rather inefficient (i.e. conservative). The load-carrying capacity predicted by the British Code is about one-fifth of the actual beam strength. According to *BS*8110, at a load which subjects the strut of the 'truss' model to a compressive stress of 5.00 N/mm^2, considering a factor of safety of 1.25, the structural member should fail. Hence, for the types of beams investigated, the failure load should never exceed 150 kN (assuming a factor of safety of 1.00, i.e. a compressive stress of 6.25 N/mm^2). Thus, for the nature of loading considered, a beam similar to *HSB*1 could never be designed, using the Code, to its flexural capacity without changing the dimensions of the member. On the other hand, in contrast to the current design methodology, the proposed method has proven very effective, since, not only are both its design and actual loads much higher than their Code counterparts, but the former pair of values (i.e. *CFP* design strength and its corresponding experimental test result) correlate very closely.

The transverse reinforcement of the type II *HSC* beam *HSB*2 has also been provided following the *CFP* provisions [7, 9], so as to be adequate to take *HSB*2 to its flexural capacity. On the other hand, the British Code predicts, in compliance with the truss-analogy concept, that beam *HSB*2 should exhibit a brittle

failure. The beam $HSB3$ was designed according to BS 8110. It is important to note, at this stage, that failure due to crushing of webs has been ignored in the design process, as it has already been found that webs of similar type I beams could sustain compressive stresses 51% higher than the value predicted by the Code. Table 4 contains the load-carrying capacities of $HSB2$ and $HSB3$ as calculated by the proposed CFP method, together with the strength values recorded from the tests, as well as the values predicted by BS 8110 and $ACI318-89$. No factor of safety was considered in the design calculations. The weakness of the Code provisions becomes clear as BS 8110 underpredicted the failure load, on both occasions, by about 25%. The predictions of $ACI318-89$ were similar to those of BS 8110. In contrast, the proposed method predicted the failure loads of both beams within an accuracy of 2%.

Some of the links of beam $HSB3$ were equipped with electrical resistance strain gauges. Figure 6 shows the load against microstrain curves obtained from the gauges fitted to the links of one of the shear spans, as well as the location of this secondary reinforcement with respect to the CFP trajectory. One leg of each of the two-legged stirrups was provided with gauges. It is apparent from the figure that the links nearest to the loading points (stirrup no 11) sustained compressive stresses instead of tensile stresses. This sheds doubt on the truss-analogy concept which professes that such a link can be modelled as a tension tie. None of the links yielded at the failure load. The average amount of micro-strain experienced by the so-called tension ties within the shear span was about 1133. The average amount of tension stress corresponding to this strain is about 227 MPa, which was only 40% of the actual yield stress of the 6 mm bars used as stirrups. The shear force carried by the shear reinforcement (V_s) according to the current Codes can be calculated as

$$v_s = A_v * f_{yv} * d/s = 56.55 * 227 * 240/75 = 41077N,$$

where A_v is area of shear reinforcement within stirrup spacing s, f_{yv} is the stress in the stirrup, and d is the effective depth of the member. Thus, considering the applied shear force at failure $V_a = V_s + V_c$, V_c becomes $(100500-41077=)59423$ N which is 3.27 times larger than the V_c value (= 18170 N) calculated using the BS 8110 equation. On the other hand, the tensile force that can be resisted by concrete alone, in compliance with the CFP concept, is equal to 46330 N [9]. According to the aforementioned concept, transverse reinforcement is needed at the junction of the model frame (Fig. 1b) to carry the tensile force in addition to the concrete capacity. The beam test results of $HSB3$, though designed to BS 8110, can be used in verifying the conditions associated with the CFP concept. The average amount of stress imposed on the links in the region where the CFP changes its direction (the 'joint') can be found by averaging the strain readings of gauges 6 to 9 (Fig. 6), which encompassed the region containing the six bars that

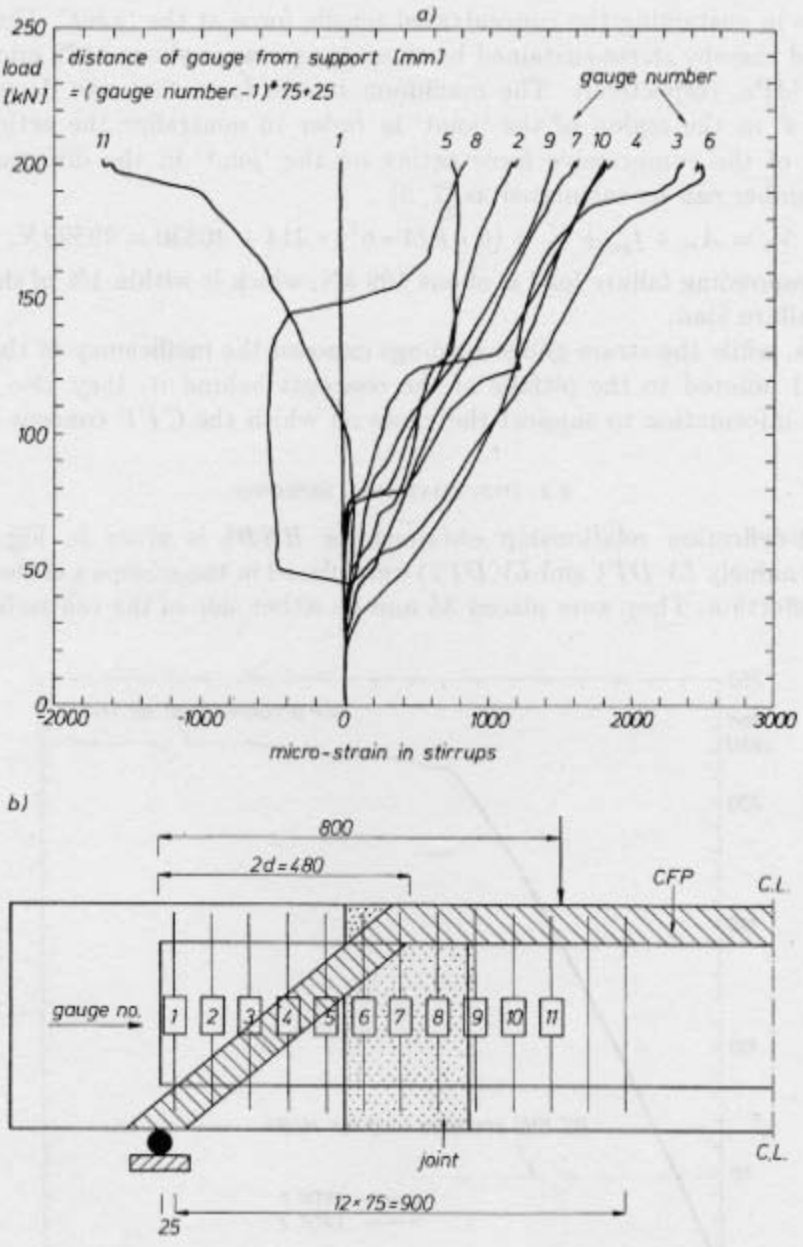

FIG. 6. (*a*) — micro-strain in the different stirrups within one of the shear spans of *HSB3*, (*b*) — stirrup/strain-gauge location with respect to the *CFP* trajectory (all dimensions in mm). Rys. 6. (*a*) — mikro-odkształcenia w różnych strzemionach w strefie ścinania w *HSB3*, (*b*) — umiejscowienie czujników na strzemionach w odniesieniu do trajektorii siły ściskającej (wszystkie wymiary w mm)

are active in sustaining the concentrated tensile force at the 'joint'. The average strain and thereby stress sustained by these gauges were about 1572 micro-strain and 314 MPa, respectively. The maximum tensile force that can develop, over a length d, in the region of the 'joint' in order to neutralize the action of the resultant of the compressive force acting on the 'joint' in the direction of the frame member can be calculated as [7, 9]

$$V_a = A_{sv} * f_{yv} + V_c = (6 * \pi/4 * 6^2) * 314 + 46330 = 99599N.$$

The corresponding failure load is about 199 kN, which is within 1% of the experimental failure load.

Thus, while the strain gauge readings exposed the inefficiency of the present Code and pointed to the pitfalls of the concepts behind it, they also recorded adequate information to support the views on which the CFP concept is based.

4.2. Deformational response

The load-deflection relationship obtained for $HSB1$ is given in Fig. 7. Two $LVDT$s (namely $LVDT1$ and $LVDT2$) were placed in the midspan of the beam to record deflection. They were placed 35 mm on either side of the centre-line of the

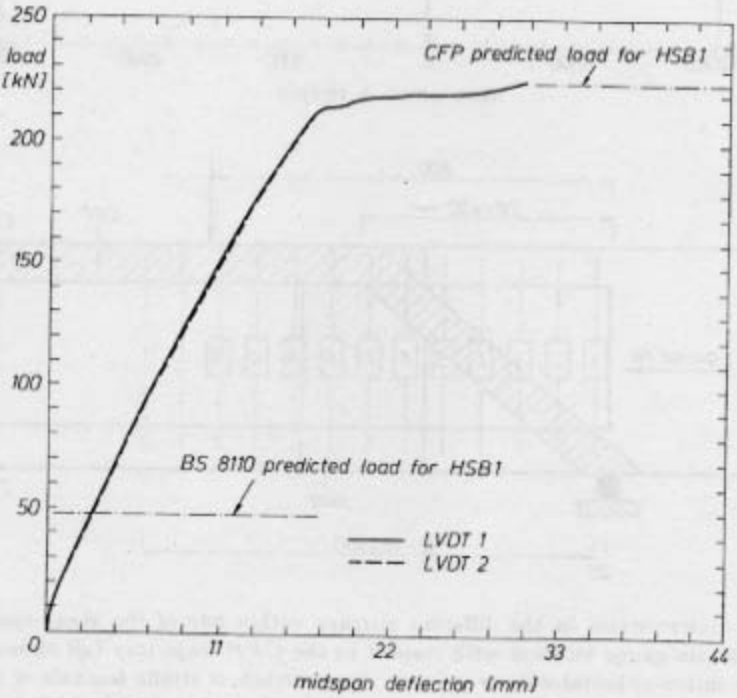

Fig. 7. Load-deflection curve of $HSB1$.
Rys. 7. Wykres obciążenie/ugięcie dla belki $HSB1$

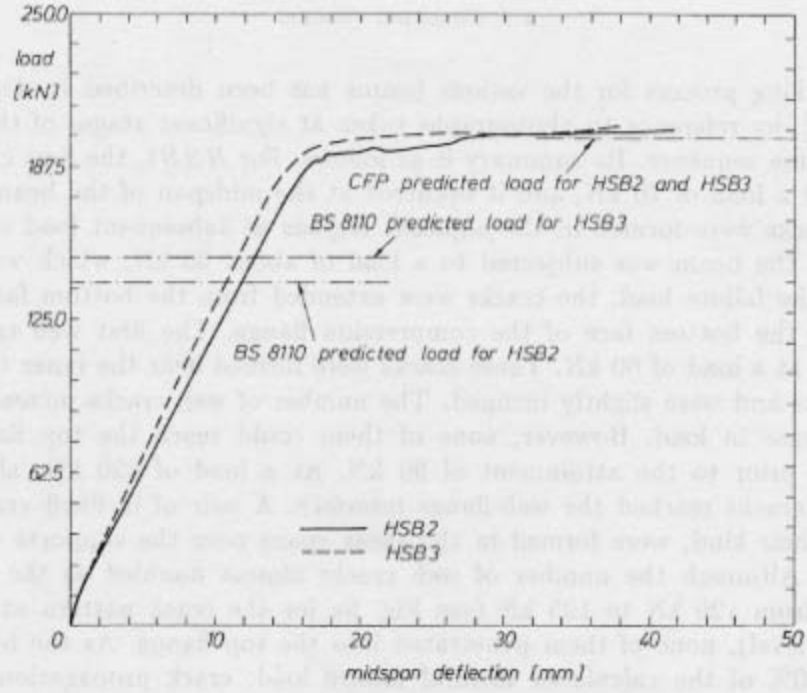

FIG. 8. Load-deflection curves of $HSB2$ and $HSB3$.
Rys. 8. Wykresy obciążenie/ugięcie dla belek $HSB2$ i $HSB3$

cross-section of the beam. The deflections recorded by both $LVDT$s are included in Fig. 7. The almost identical nature of the load-deflection curves monitored by the $LVDT$s demonstrates that the loading was truly vertical, and uniformly distributed across the width of the beam. The absence of any torsional moment in the midspan is also evident. The load-carrying capacity predicted by the different methods has been shown in Fig. 7 for comparison purposes. The ductile nature of the load-deflection curve points to the flexural mode of failure.

The load-deflection relationships of $HSB2$ and $HSB3$ are shown in Fig. 8. Although two $LVDT$s (70 mm apart) recorded the midspan deflection of either of the beams, only readings of one of them have been shown in the figure, as they were almost identical. The load-carrying capacity predicted by different design methods has also been included in Fig. 8. It appears from the figure that both the beams underwent ductile deformation at failure. The deformational response of $HSB3$ was slightly stiffer than that of $HSB2$, probably because of the additional amount of web reinforcement. However, at loads near to failure, both of them exhibited very much similar responses. This similarity indicates that the provision of 60% more web reinforcement in $HSB3$ did not result in any improved performance in comparison to $HSB2$.

4.3. CRACKING PROCESS

The cracking process for the various beams has been described in detail elsewhere [9], by reference to photographs taken at significant stages of the crack-propagation sequence. Its summary is as follows. For $HSB1$, the first crack was visible at a load of 20 kN, and it occurred at the midspan of the beam. A few more cracks were formed in the adjacent regions at subsequent load steps. By the time the beam was subjected to a load of about 50 kN, which was about 22% of the failure load, the cracks were extended from the bottom face of the beam to the bottom face of the compression flange. The first web crack was detected at a load of 60 kN. These cracks were formed near the inner two loading points and were slightly inclined. The number of web cracks increased with the increase in load. However, none of them could reach the top flange-web interface prior to the attainment of 90 kN. At a load of 120 kN, almost all the web cracks reached the web-flange interface. A pair of inclined cracks, the first of their kind, were formed in the shear spans near the supports at about 150 kN. Although the number of web cracks almost doubled as the load increased from 120 kN to 195 kN (see Fig. 9a for the crack pattern at the latter load level), none of them penetrated into the top flange. As the beam was within 10% of the calculated flexural failure load, crack propagation was no longer marked after this stage until failure, due to safety reasons. A steady increase in deflection was noticeable from the load of 215 kN. The flexural cracks were widening gradually with increasing load. The beam underwent a flexural failure at an applied load of 225 kN, when the vertical cracks of the constant-moment flexural span penetrated deep into the flange. At failure, horizontal cracks were visible in the top flange (i.e. compression flange) and spalling of concrete at the top surface also took place. Figure 9b shows the beam after failure. It is important to note that, not even a single shear crack, from any part of the beam, could penetrate the compression flange at or before the final failure.

The cracking processes exhibited by $HSB2$ and $HSB3$ were similar. For instance, typical late stages of these processes are shown in Fig. 10, by reference to data obtained for $HSB3$. The crack patterns for both beams in the region where failure occurred appear in Fig. 11.

In $HSB2$, the first crack was visible in the midspan of the beam at a load of 25 kN. More flexural cracks were formed in the subsequent load steps. By the time about 30% of the failure load was applied, most of the flexural cracks almost reached the top flange-web interface. The first web crack was also detectable at this stage. More shear cracks were formed in the subsequent load steps. At about 45% of the failure load, one of the shear cracks penetrated a little into the flange. This crack penetrated half way into the flange at a load of 150 kN, which was 75%

a)

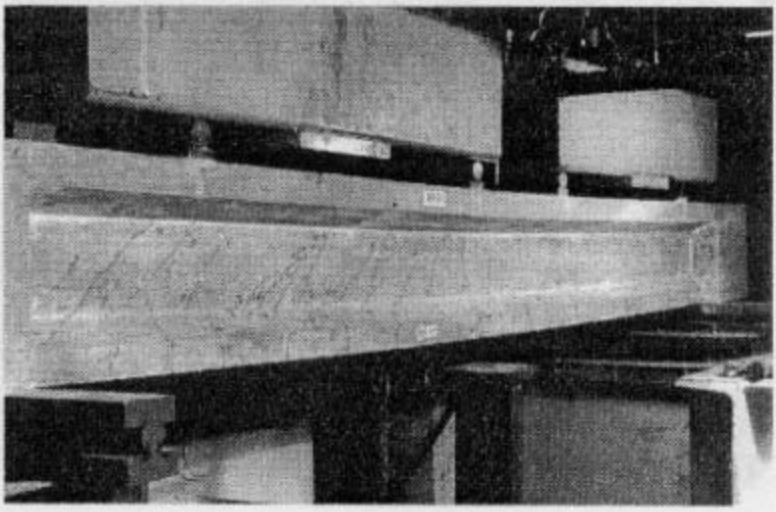

195 kN

b)

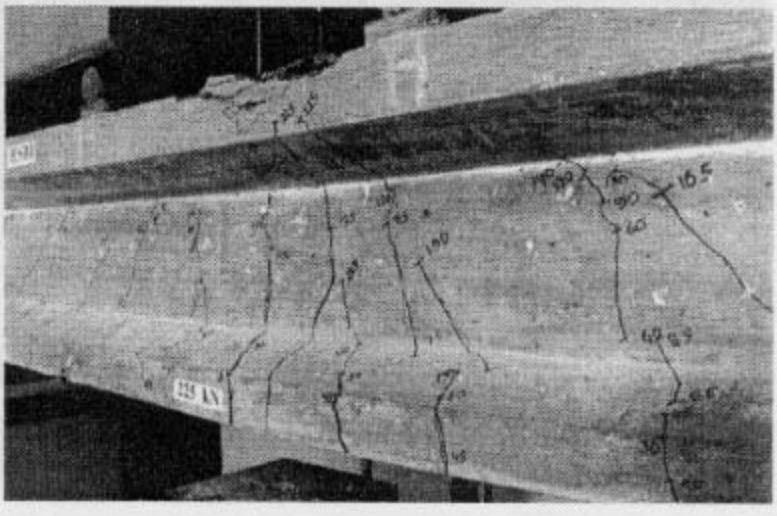

225 kN

FIG. 9. The latter stages of the cracking process exhibited by $HSB1$ during its test to failure; (a) — 195 kN; (b) — 225 kN.

Rys. 9. Końcowe stadia procesu zarysowania zachodzące w belce $HSB1$ w trakcie badania na zniszczenie; (a) — przy 195 kN, (b) — przy 225 kN

a)

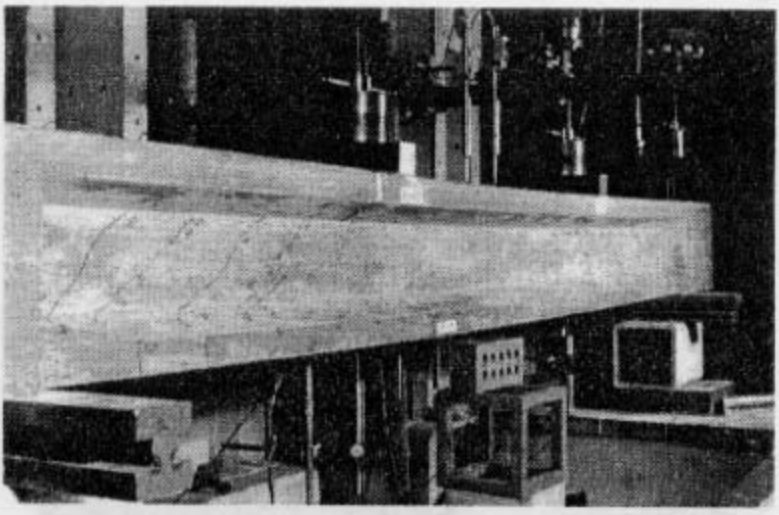

180 kN

b)

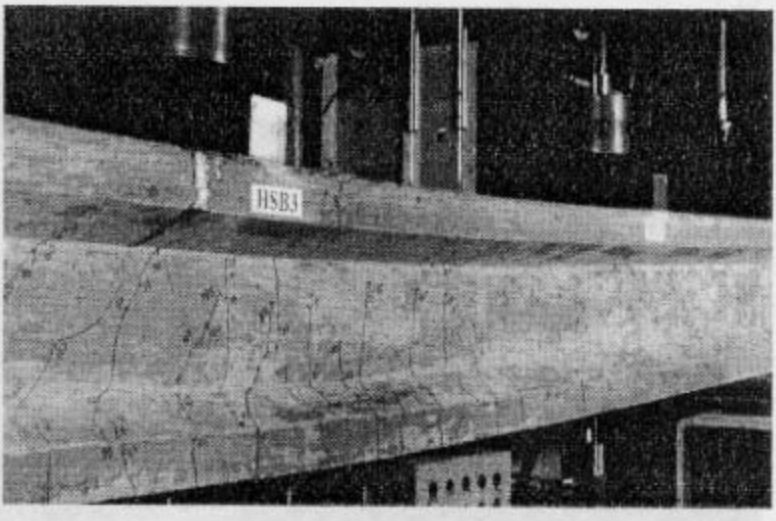

200 kN

FIG. 10. The latter stages of the cracking process exhibited by *HSB3* during its test to failure; (*a*) — 180 kN; (*b*) — 200 kN.

Rys. 10. Końcowe stadia procesu zarysowania zachodzące w belce *HSB3* w trakcie badania na zniszczenie; (*a*) — przy 180 kN, (*b*) — przy 200 kN

a) b)

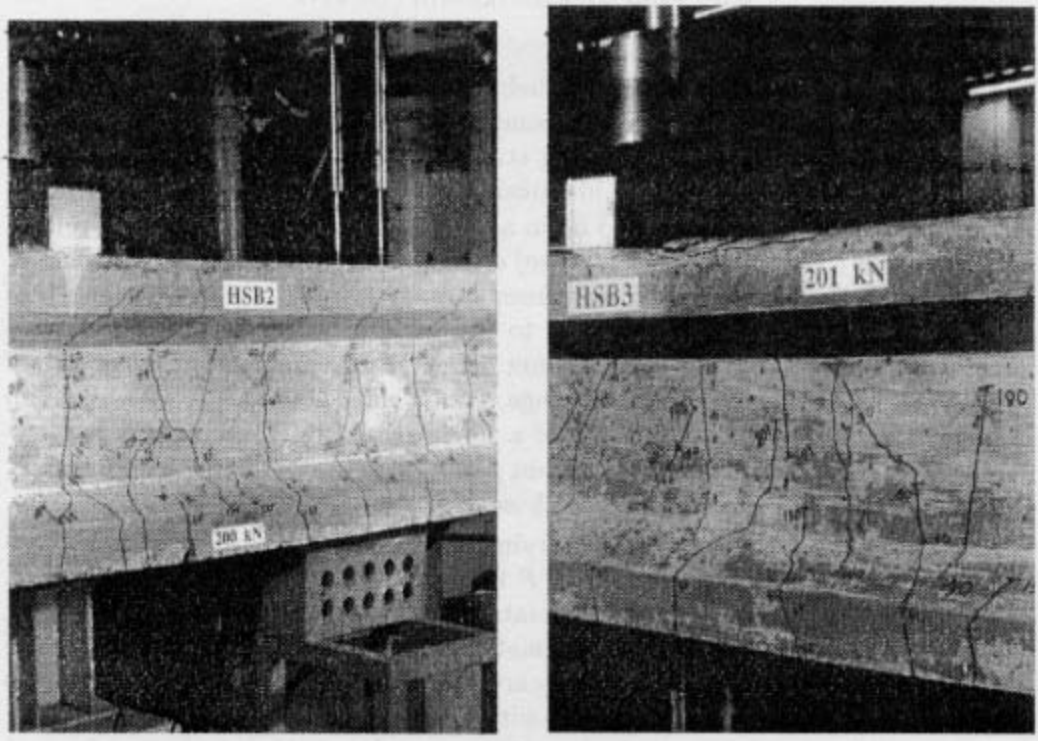

FIG. 11. Crack patterns in the region where failure occurred in (*a*)—*HSB2* and (*b*)—*HSB3*.
Rys. 11. Przebieg rys w miejscu zniszczenia; (*a*) — w belce *HSB2* oraz (*b*) — w belce *HSB3*

of the failure load. After the application of loads a little above 90% of the failure load, the crack propagation was almost stabilized. By about 95% of the failure load, one of the inclined cracks penetrated deep into the flange (see Fig. 11a). (The penetration of the shear crack into the flange for *HSB2* is in contrast to the lack of such penetration in the case of *HSB1*; one likely reason for this is that the two-point loading combination results in maximum moment and shear occurring near the point loads (where penetration of shear cracks into the flange occurs), whereas for the four-point loading the maximum values of moment and shear are not coincident.) At about 200 kN, failure eventually occurred due to the failure of the compressive zone near the loading points.

Although the cracking process in *HSB3* was similar to that observed in *HSB2*, the formation of the first web crack and its penetration into the top flange was slightly delayed in comparison to *HSB2*. The mechanism of failure of *HSB3* was also similar to that of *HSB2*. Figure 11b shows the horizontal cracks formed in the top flange of the beam, at a section very near to the loading point within the flexural span.

4.4. COMPARISON OF TEST RESULTS WITH SIMILAR BEAMS MADE FROM NORMAL-STRENGTH CONCRETE

The effect of concrete strength on the behaviour of *RC* members at the ultimate limit state can best be understood by comparing test results of similar beams but made from concrete of widely differing strengths. The beams *C* and *B* reported by KOTSOVOS and LEFAS [7] were identical, respectively, to the type I *HSC* beam *HSB*1 and type II *HSC* beam *HSB*2 in all respects other than concrete strength and properties (i.e. strength and bar size) of some of the transverse reinforcement. The former beams were constructed from a *NSC* mix with a cube strength of about 40 MPa. Again, in comparison to the 1.5 mm diameter transverse reinforcement of *HSB*1, beam *C* had 1.6 mm diameter links having yield strength of 360 MPa. The horizontal leg of the flange reinforcement in beam *B* was made up from two unconnected hoops in lieu of a single two-legged link around the perimeter of the top flange. The arrangement and spacing of transverse reinforcement of beams *C* and *B*, otherwise, follow those of *HSB*1 and *HSB*2 in Fig. 4.

As for beam *HSB*1, the load-carrying capacity of beam *C* was much more closely predicted by the concept of *CFP* than by the available Codes of practice. The British Code *BS* 8110 underestimated the load-carrying capacity by 81%, while the proposed method underestimated it by only 6.87%. For *HSB*1, the British Code underestimates the load-carrying capacity by 79.2%. However, the proposed method predicts the capacity with almost no underestimation. For beam *C*, the actual flexural failure took place 15% above the calculated (design) flexural capacity of the (critical) cross-section. This phenomenon will be explained while describing the causes of observed behaviour and failure mechanism. On the other hand, for *HSB*1, the experimental failure took place almost at the calculated flexural capacity. The load-deflection relationships of beam *C* and *HSB*1 are compared in Fig. 12. As can be seen from the figure, both beams exhibited ductile deformational behaviour and, interestingly, similar stiffness and strength. The load-deflection curve of *HSB*1 was a little less stiff than that for beam *C*. The initial stages of the cracking process of beam *C* were similar to those of *HSB*1. A significant difference in the above process was detectable at a later stage. In beam *C*, the rate of crack extension was significantly reduced as the load increased beyond a level approximately equal to half the failure load. In the case of *HSB*1, on the other hand, even though cracks could not penetrate into the compression flange until very near to failure, new cracks were formed up to about 90% of the failure load. In beam *C*, the cause of failure appears to have been the 'snapping' of the flange hoop reinforcement, which was designed to sustain a tensile force about 15% lower than the actual failure load. Although in the case of beam *C*, (quasi-) ductile behaviour was exhibited, it would appear that underestimating the true flexural capacity (though safe from the failure-load standpoint) may lead to types

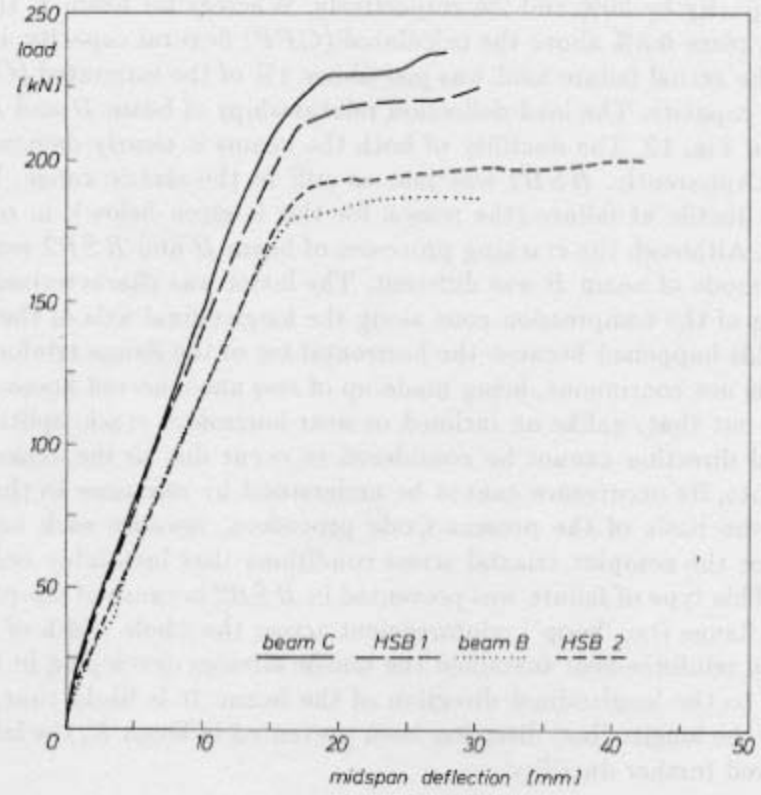

FIG. 12. Comparison of experimental load-deflection curves of normal- ($f_{cu} \sim 40$ N/mm^2) and high- ($f_{cu} \sim 80$ N/mm^2) strength beams: $HSB1$ and beam C; and $HSB2$ and beam B.
Rys. 12. Porównanie doświadczalnych wykresów obciążenie/ugięcie dotyczące belek z betonu zwykłego ($f_{cu} \sim 40$ N/mm) i betonu o dużej wytrzymałości ($f_{cu} \sim 80$ N/mm): $HSB1$ i C oraz $HSB2$ i B

of failure other than flexural (as, for example, due to the amount of transverse reinforcement being lower — as in the case of flange hoop reinforcement above — than actually required); such failures may be brittle in nature and thus not give adequate warning of the impending collapse. In the case of $HSB1$, the flexural capacity was not underestimated. Consequently, the flange reinforcement could espace snapping, although the member's ductility was not appreciably larger than that of beam C.

The load-carrying capacity of beam B, like that of beam $HSB2$, was also more closely predicted by the proposed concept than by the available Codes of practice. The British Code *BS* 8110 and the American Code *ACI* 318-89 underestimated the load-carrying capacity of beam B by 38% and 42% respectively. For $HSB2$, the British Code and the proposed method underestimated the load-

carrying capacity by 30% and 2% respectively. Whereas for beam B the flexural failure took place 6.3% above the calculated (CFP) flexural capacity, in the case of $HSB2$ the actual failure load was just above 1% of the estimated (CFP) flexural failure capacity. The load-deflection relationships of beam B and $HSB2$ are compared in Fig. 12. The ductility of both the beams is clearly demonstrated in the figure. Apparently, $HSB2$ was just as stiff in the elastic range, but somewhat more ductile at failure (the reason for this is given below), in comparison to beam B. Although the cracking processes of beam B and $HSB2$ were similar, the failure mode of beam B was different. The latter was characterized by vertical splitting of the compression zone along the longitudinal axis of the beam [7]. However, this happened because the horizontal leg of the flange reinforcement in beam B was not continuous, being made up of two unconnected hoops. It should be pointed out that, unlike an inclined or near-horizontal crack, splitting in the longitudinal direction cannot be considered to occur due to the action of shear forces. In fact, its occurrence cannot be understood by reference to the concepts that form the basis of the present Code provisions, because such concepts do not cater for the complex triaxial stress conditions that invariably occur in RC members. This type of failure was prevented in $HSB2$ because of the provision of continuous flange (i.e. 'hoop') reinforcement across the whole width of the beam, as this hoop reinforcement sustained the tensile stresses developing in the flange, orthogonal to the longitudinal direction of the beam. It is likely that, had such splitting in the longitudinal direction been prevented in beam B, the latter would have achieved further ductility.

4.5. CAUSES OF OBSERVED BEHAVIOUR AND FAILURE MECHANISM

It is clear from the previous sections that the straightforward extension of the proposed physical model, based on the concept of CFP as applied previously to the design of RC beams made from NSC, also leads, in the case of the HSC beam $HSB1$, to a design solution which is both efficient and safe. Nevertheless, two aspects raised above, call for explanation. First, while in beam C the propagation of cracks almost stopped at a load in the neighbourhood of half the failure load, in $HSB1$ the formation of new cracks was continued until the beam sustained a load close to 90% of the failure load. A possible explanation for this might be argued for as follows. The flexural capacities of $HSB1$ and beam C were almost identical. High-strength concrete, due to its higher stiffness (at the material level), experiences less volume dilation at a load level near to failure than normal-strength concrete. Now, it is due to this volume dilation that a triaxial compressive state of stress can occur in localized regions in the compressive zone. Thus, the effect of triaxial stresses should be less pronounced in a HSC beam in comparison to a similar NSC beam. This is what actually happened in the tests,

where the degree of triaxiality was higher for the *NSC* beam and hence crack propagation was inhibited more than in its *HSC* counterpart. In addition, near failure, the location of the neutral axis of the *HSC* member was considerably closer to the top fibres than in the case of the *NSC* girder.

The second point requiring explanation concerns the fact that the failure load could be predicted more closely for the case of the beam *HSB*1 than for beam *C*. As already mentioned, beam *C* withstood a load about 15% higher than the calculated flexural load (the latter being based on uniaxial properties). It can be shown, by simple calculation, that concrete, at the maximum moment section, in the compression zone was subjected to a stress much higher than its uniaxial cylinder strength (and this increases the lever arm by about 15%, assuming, of course, that the main reinforcement did not simultaneously exhibit a higher stress than its characteristic strength). On the other hand, the uniaxial cylinder strength in the case of *HSB*1 was already of the order of twice that of beam *C* and, while beam *HSB*1 failed in flexure, no appreciable enhancement in the load-carrying capacity could be noticed at failure due to the much less pronounced effect of triaxiality. It can be seen from the simplified stress block of Fig. 13 that the lever

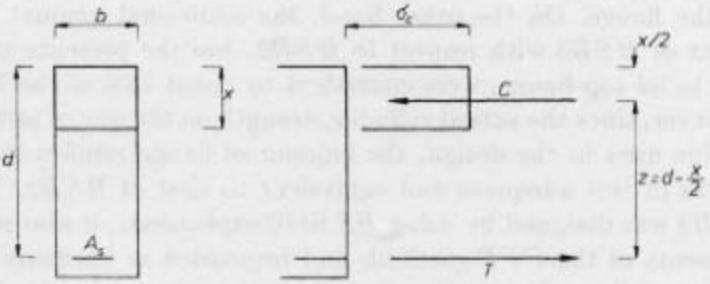

$$M_f = T.z = C.z,$$

where $C = b \times \sigma_c$, f_{cyl} = cylinder concrete strength,
$T = A_s f_y$, f_{cu} = cube concrete (characteristic) strength,
$\sigma_c = 0.8 f_{cyl} = 0.64 \sim 0.67 f_{cu}$, f_y = characteristic strength of tension steel.

FIG. 13. Simplified stress block.
Rys. 13. Uproszczony wykres naprężeń

arm z, used in the calculation of the moment-carrying capacity M_f, is affected by the strength of concrete from which the member is made. Thus, the value of z for *HSB*1 was initially higher than that of beam *C*. Moreover, due to the smaller effect of triaxiality in *HSC* members, there was very little scope for the lever arm of *HSB*1 to increase its length further. Consequently, while beam *C* could experience some gain in load-carrying capacity as a result of the beneficial effect of triaxiality, hence attaining a failure load higher than the load calculated on the basis of its uniaxial cylinder strength, beam *HSB*1 failed to achieve such a gain.

Of course, volume dilation did take place at the ultimate limit state of *HSB1*; and, as for *NSC* members, at loads near to failure, such a dilation induces 'critical' tensile stresses adjacent to the flexural crack-tip regions which were subjected to the maximum compressive stress intensity. Figure 9b clearly demonstrates the presence of such tensile stresses at failure (see the horizontal crack near the top surface), which eventually gave rise to compression/tension state of stress. As a result of this, reduction of concrete strength in the longitudinal direction and eventual collapse due to horizontal splitting and spalling of concrete at top flange (the compressive zone) of the beam, in the flexural span, took place.

The behaviour of type II *HSC* beams at the ultimate limit state was very much in line with the behaviour of type I *HSC* beam, as were their respective relationship to the *NSC* beams. Thus the causes of the observer behaviour of type I beam *HSB1* as explained above can be considered to be applicable to type II beams (*HSB2* and *HSB3*) as well. However, the resemblance of *HSB2* and *HSB3* in the cracking, deformational and failure processes deserves explanation. The basic difference in the design of *HSB2* and *HSB3* was in the amount of web reinforcement and in the presence or absence of flange reinforcement. On the one hand, *HSB3* had 60% more web reinforcement and total absence of links in the flange. On the other hand, the additional amount of transverse reinforcement of *HSB3* with respect to *HSB2*, and the presence of nominal reinforcement in its top flange, were equivalent to about 75% of the flange links of *HSB2*. However, since the actual cylinder strength on the day of testing was more than the value used in the design, the amount of flange reinforcement available to *HSB3* was in fact adequate and equivalent to that of *HSB2*. Therefore, although *HSB3* was designed by using *BS* 8110 expressions, it also nearly fulfilled the requirements of the *CFP* method, and responded in harmony with *HSB2*, when tested to failure. It is interesting to note that, neither in *HSB2* nor in *HSB3*, the strut of the 'truss' model failed in compression as predicted by the British Code *BS* 8110. Thus, the inadequacy of the 'truss' model is, once again, exposed.

5. ANALYTICAL INVESTIGATION ON THE ROLE OF FLANGE REINFORCEMENT

It has been pointed out that the role of flange reinforcement is to contribute to the ductility of an *RC* structure and not to the load-bearing capacity of the member [7]. In an *RC* member made from *NSC*, flange reinforcement probably plays an instrumental role in confining the top flange, thereby increasing the strength of the compressive zone. This usually deters premature propagation of cracks into the flange and, thereby, aids in preventing violent collapse without warning. However, in the case of *HSC* members, the possibility that flange reinforcement

acts differently should be considered on account of the very reduced degree of triaxiality in such members.

Although it may be unwise to reach a general conclusion without performing extensive experimentation, a limited numerical parametric study on *HSC* beams without flange reinforcement might throw some light on the understanding of *HSC* beam behaviour. With this end in view, two beams, *HSB*4 and *HSB*5, were numerically tested using the reliable three-dimensional (3-*D*) finite element (*FE*) model [20–22] which adopts a brittle constitutive relationship at the material level. The features of *HSB*4 and *HSB*5 are identical to *HSB*1 and *HSB*2, respectively, in all respects except flange reinforcements, which were non-existent. Since detailed description of the *FE* modelling (i.e. *FE* discretization, analytical crack patterns, load-deformational behaviour) of *HSB*1 and *HSB*2 along with the extension of the generality of the 3-*D FE* model to *HSC* mixes are available elsewhere [23], they are not included here.

The plotting convention, which has been described in detail elsewhere [20–23], can be briefly summarized at this point. Plots are superimposed onto the mesh lying on a plane parallel to the reference plane (*XZ*). In the present study only one-fourth of the members were analysed due to the relevant symmetries. The longitudinal beam section is the reference plane. The symbols for the various cracks at the relevant Gauss points are as follows. Oriented dashes represent the intersection of a crack plane with the plotting plane *XZ* whenever the angle subtended between these two planes exceeds 45°. Should both planes form an angle smaller than 45°, the crack plane is indicated by a circle. Three cracks at the same Gauss point are indicated by an asterisk.

The ultimate load-carrying capacities of *HSB*4 and *HSB*5 were found to be equal to the load-carrying capacities of *HSB*1 and *HSB*2, respectively, signifying the apparently negligible role of flange reinforcement in the overall failure load of a member. The load-deflection curves of the beams without flange reinforcement were identical to their counterparts with flange reinforcement (the deflections at the ultimate failure load in beams without flange reinforcement being trivially smaller than their counterparts). The initial stages of the cracking process of *HSB*4 and *HSB*5 were also found to be very much akin to those of *HSB*1 and *HSB*2, respectively.

In Fig. 14, the analytical crack patterns of the last two converged load steps of the nonlinear analyses of *HSB*1 and *HSB*4 have been shown (previous load steps are identical). It can be seen from the figure that, at the load of 218.88 kN, the top flange of *HSB*4 was subjected to more extensive cracking. The occurrence of a near-horizontal additional crack at the top-most Gauss point in the element nearest to the loading point close to the support and complete loss of stiffness (marked by an asterisk) at another Gauss point in the same element, clearly demonstrates that, in the absence of flange reinforcement, cracks can penetrate

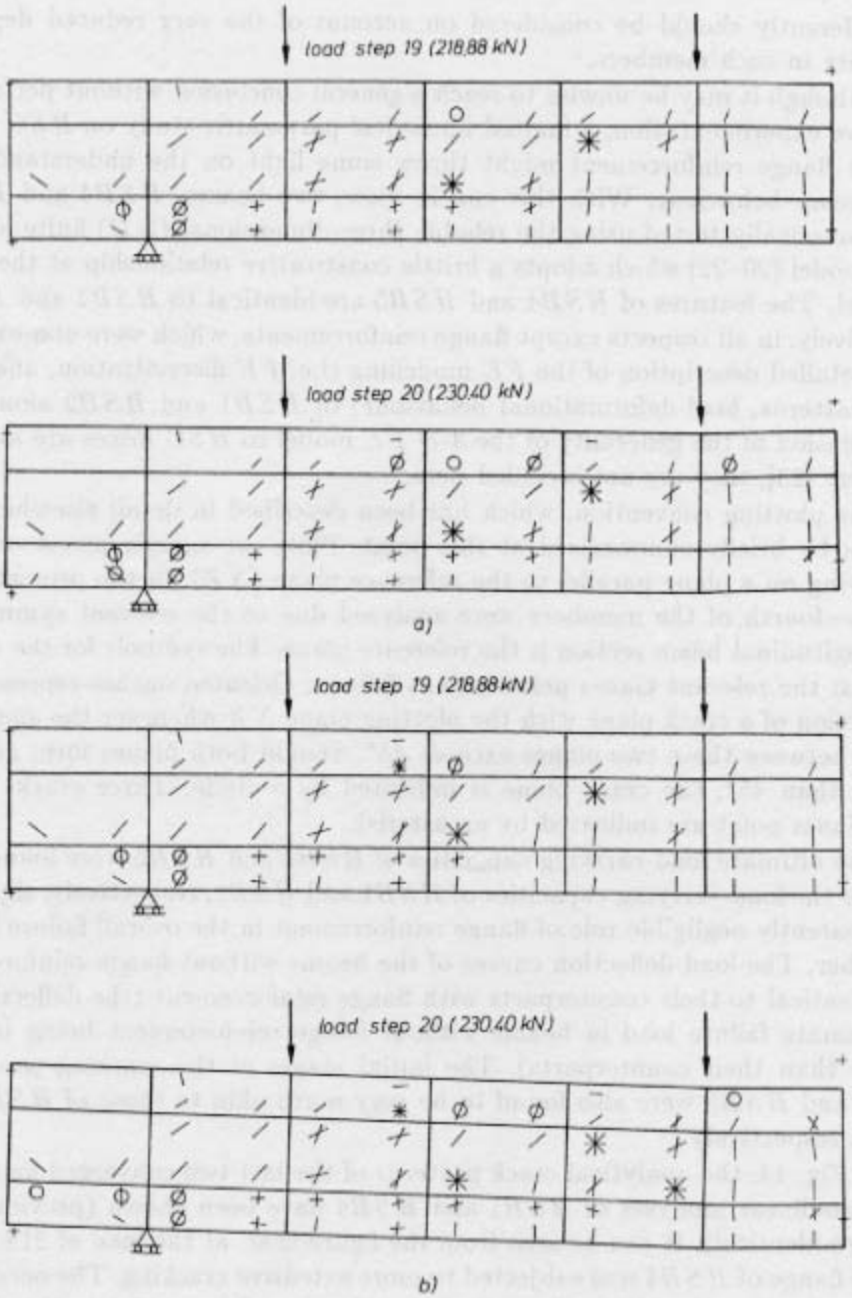

FIG. 14. Analytical crack patterns at the last two converged load steps of (*a*) — *HSB*1 and (*b*) — *HSB*4.

Rys. 14. Przebieg rys uzyskany drogą analityczną, dotyczący dwóch ostatnich kroków obciążenia, (*a*) — dla belki *HSB*1, (*b*) — dla belki *HSB*4

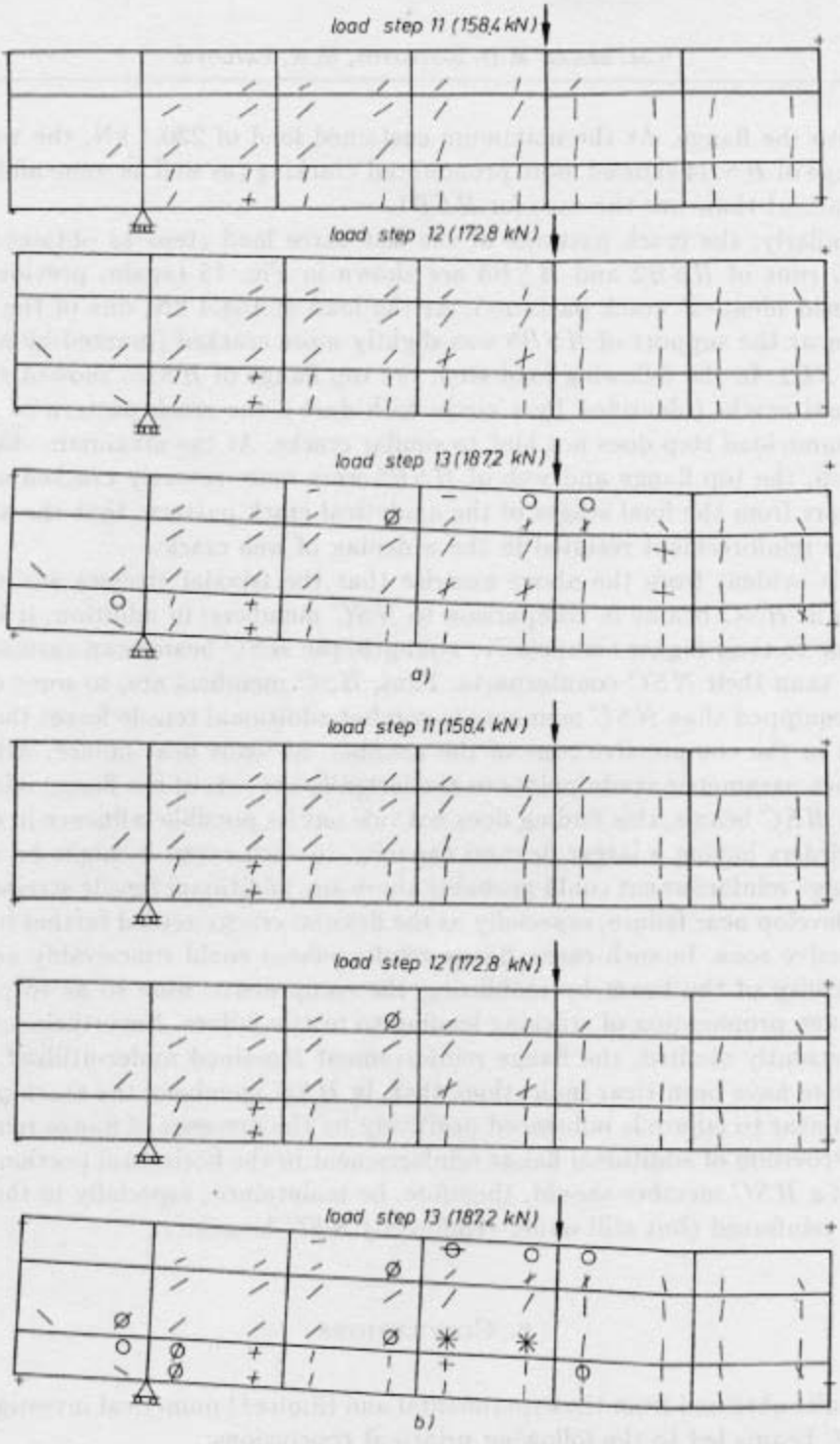

FIG. 15. Analytical crack patterns at the last three converged load steps of (*a*) — *HSB2* and (*b*) — *HSB5*.

Rys. 15. Przebieg rys uzyskany drogą analityczną, dotyczący trzech ostatnich kroków obciążenia (*a*) — dla belki *HSB2* — (*b*) dla belki *HSB5*

deep into the flange. At the maximum sustained load of 230.4 kN, the web and top flange of $HSB4$ showed more pronounced cracking (as well as some additional deformation) than was the case for $HSB1$.

Similarly, the crack patterns of the last three load steps as obtained from the FE runs of $HSB2$ and $HSB5$ are shown in Fig. 15 (again, previous load steps yield identical crack patterns). At the load of 158.4 kN, one of the Gauss points near the support of $HSB5$ was slightly more cracked (marked by a cross) than $HSB2$. In the following load step, the top flange of $HSB5$ showed signs of additional cracks (identified by a circle with dash); the crack pattern of $HSB2$ at the same load step does not hint to similar cracks. At the maximum sustained load step, the top flange and web of $HSB5$ were more severely cracked as well. It appears from the final stages of the analytical crack pattern, that the absence of flange reinforcement resulted in the widening of web cracks.

It is evident from the above exercise that the triaxial stresses are less noticeable in HSC beams in comparison to NSC members; in addition, it is clear that, due to their higher compressive strength, the HSC beams can sustain more tension than their NSC counterparts. Thus, HSC members are, to some extent, better equipped than NSC members to combat additional tensile forces that may develop in the compressive zone of the member, at loads near failure. Although the above parametric study points to the insignificant role of the flange reinforcement in HSC beams, this finding does not rule out its possible influence in similar HSC girders having a larger flexural capacity. In such cases, it might be argued that flange reinforcement could probably share any additional tensile stresses that might develop near failure, especially as the flexural cracks extend further into the compressive zone. In such cases, flange reinforcement could conceivably enhance the ductility of the beam by mobilizing the compressive zone so as to prevent the sudden propagation of cracking leading to brittle failure. Nevertheless, in the cases presently studied, the flange reinforcement remained under-utilized. However, there have been clear indications that, in HSC members, the crack pattern at loads near to failure is influenced positively by the presence of flange reinforcement. Provision of additional flange reinforcement in the horizontal portion of the CFP of a HSC member should, therefore, be maintained, especially in the more heavily reinforced (but still under-reinforced) HSC beams.

6. CONCLUSIONS

The results obtained from the experimental and (limited) numerical investigations on HSC beams led to the following principal conclusions:

a. The recognition of the multiaxial effects that govern load-carrying capacity in the region of the path along which the compressive force is transmitted from

the loading points to the supports, and the fact that the concept of *CFP* can be suitably used in the design and understanding of the behaviour of *HSC* beams, appear to point towards a simple and rational design procedure for *RC* members made from a wide range of concrete strength. The latter unifying feature, therefore, does not require the design procedure to be modified in accordance to material strength as it encompasses both *NSC* and *HSC* members. (In the present set of *HSC* beams the main reinforcement adopted (2*Y*20) was the same as that for the earlier *NSC* beam series in order to attain similar flexural capacities that enable a comparison between *HSC* and *NSC* members to be made, it is obvious that a larger flexural capacity could be achieved by the *HSC* members with additional longitudinal reinforcement — say 3*Y*20.)

b. The British Code *BS* 8110, like other current Codes, underestimated grossly (by about 80%) the load-carrying capacity of the type I *HSC* beam tested. The reason for this is that the Code overestimates the significance of the contribution of the web to shear capacity while it underestimates the contribution of the flange. Thus, whereas current code rules lead to the conclusion that such a member must fail in shear due to, apparently, insufficient transverse reinforcement, flexural failure was in fact achieved experimentally (as for the other two beams), a finding correctly predicted by the *CFP* method of design, showing that code requirements may sometimes specify larger amounts of transverse reinforcement than actually needed.

c. Underestimation of flexural capacity of a member — though 'safe' — may lead the structure to exhibit a brittle type of failure.

d. A structural member undergoing flexural failure shows a considerable amount of dilation of concrete in the compressive zone subjected to flexural stresses. This dilation, however, is less pronounced in a *HSC* beam in comparison to a similar *NSC* member. Interestingly, the higher stiffness and smaller volume dilation of *HSC*, when compared to *NSC* at the material level, do not seem to have significantly affected — in the present, admittedly limited, study — the stiffness and ductility of corresponding *HSC* and *NSC* beams at the structural level. Because of the adoption of the same longitudinal-reinforcement detailing (see *a* above) and the resulting flexural-failure type, even the failure loads are similar for equivalent members made of *HSC* and *NSC*, except that, in the former, cracking is delayed (although the final crack patterns are also similar).

e. The pronounced triaxiality of *NSC* members results in an *additional, hidden* margin of safety against flexural failure; such a margin of safety may, in fact, lead to a brittle mode of failure, due to other causes (e.g. shear), which design procedures aim to delay until flexural failure occurs first. On the other hand, the significantly less pronounced triaxiality of *HSC* members eliminates the above hidden margin of safety; moreover, for a sufficiently high concrete strength the

dynamic aspect of the cracking process — a dominant feature of *HSC* — may possibly lead to a further reduction in flexural capacity which, in turn, could result in an unsafe design solution. These conclusions are perforce of a tentative nature, but it is evident that further research in this area is needed as the design implications are considerable.

f. The 'truss' model does not explain structural concrete behaviour adequately. Although the type II beam designed to *BS* 8110 formulae (after ignoring the possible failure of the compressive 'strut') attained its flexural capacity, it was an uneconomical solution, since it contained about 60% higher transverse reinforcement than a similar beam designed to the *CFP* concept. It is important to note that none of the *HSC* members tested failed due to crushing of concrete 'struts', the latter being an important feature of the British Code provisions for shear. It is apparent, therefore, that revision of Codes without reviewing the concepts that form the basis of these Codes cannot lead to improvements. The over-increasing number of design equations, based on traditional concepts, put forward by various researchers, portray the difficulties invariably associated with such concepts.

g. The concrete contribution to the shear-carrying capacity of the type II *HSC* beam designed using the *BS* 8110 formulae, as demonstrated from stirrup strain readings, was greatly underpredicted by the British Code. The strain readings of the same beam, when employed in calculating the amount of tensile force at locations where the path changes direction, can lead to quite accurate estimates of *CFP* predictions.

h. A limited parametric study suggests that the role of flange reinforcement in a *HSC* beam is less important than in a *NSC* beam, and such an observation is backed by available experimental evidence (see the comparative behaviours of beams *C* and *HSB*1 described in this paper). This, of course, is to be expected from the reduced degree of triaxiality of the *HSC* materials, a fact automatically allowed for by the constitutive model and related *FE* package which, like the *CFP* concept, are equally applicable to both *NSC* and *HSC* structures.

Acknowledgements

The first author would like to express his gratitude to The Association of Commonwealth Universities, UK, for awarding him a Commonwealth Scholarship to carry out research of which the present work forms part, and to Bangladesh University of Engineering and Technology for granting him leave of absence during this research programme.

APPENDIX A. DESIGN CALCULATIONS FOR *HSB1*

Flexural capacity (see Fig. 2)

$A_s = 628.32$ mm^2, and $f_y = 560$ N/mm^2 gives $T = 351859.2$ N,
$f_{cu} = 80$ N/mm^2 gives $\sigma_c = 0.67\, f_{cu} = 53.6$ N/mm^2.
Since $C = T$, $A_c = 351859.2/53.6 = 6564.5$ mm^2.
Thus $X = 33$ mm and $Xg = 16.5$ mm.
Lever arm, $z = 240 - 16.5 = 223.5$ mm.
Hence flexural capacity $M_f = 351859.2 * 223.5 = 78640531.2$ Nmm.
Maximum sustained four-point load as indicated in Fig. 3a is $4 * 56171.8$ N.

Shear force sustained by concrete

According to the *CFP* method (see Refs [7] and [9]), the moment corresponding to the failure load (in Nmm) is given by

$$M_c = 0.875sd\left(0.342b_1 + 0.3\frac{M_f}{d^2}\sqrt{\frac{z}{s}}\right)\sqrt[4]{\frac{16.66}{\rho_w f_y}}, \tag{A.1}$$

where the various parameters are defined in Notation and in Fig. A1.

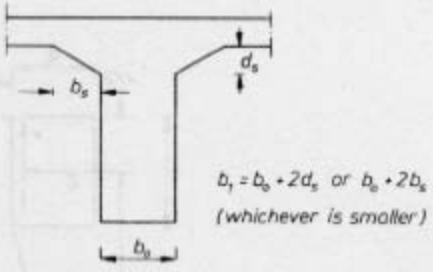

FIG. A1. Definition of b_1 in Equation A.1.
Rys. A1. Definicja b_1 w równaniu A.1

The tensile force that can be resisted by concrete alone in the region where the path changes its direction (in N) is given by

$$V_c = M_c/s. \tag{A.2}$$

There are two possible shapes of compressive force path as indicated in Fig. A2.

PATH 1: Shear span $s = 300$ mm ($< 2d = 480$ mm and $> d = 240$ mm) as shown in Fig. A2a. Thus we assess M_c by assessing M_c for $s = 480$ mm and $s = 240$ mm and M_c for $s = 300$ mm is obtained by linear interpolation.
For $s = 480$ mm, from Eq. (A.1), $M_c = 27751708.8$ Nmm.
For $s = 240$ mm, $M_c = M_f = 78640531.2$ Nmm.

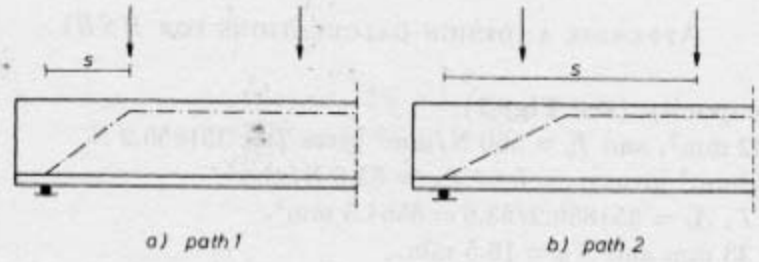

FIG. A2. Possible shapes of the compressive-force path.
Rys. A2. Możliwe drogi przebiegu siły ściskającej

By interpolation, for $s = 300$ mm, $M_c = 78640531.2 - (78640531.2 - 27751708.8) * 60/240 = 65918325$ Nmm. However applied bending moment at $s = 300$ mm, $M_a = 33703080$ Nmm $\ll 65918325$ Nmm. Thus, for this path transverse reinforcement is not required.

PATH 2: Shear span $s = 1100$ mm, as shown in Fig. A2b.
Using Equations A.1 and A.2, $M_c = 44572133.4$ Nmm and $V_c = 44572133.4/1100 = 40520.12$ N. Applied shear force $V_a = 56171.80$ N > 40520.12 N. Thus this path is more critical and shear reinforcement is required.

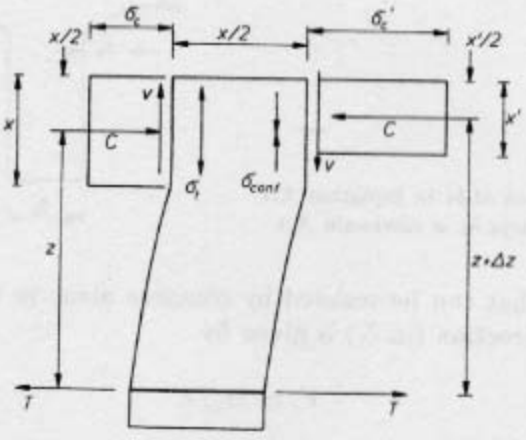

FIG. A3. Assessment of excess tension due to bond failure.
Rys. A3. Ocena dodatkowego rozciągania, spowodowanego utratą przyczepności

Transverse reinforcement

(i) For excess tension due to change in path direction (see Refs [7] and [9]) $T_{sv} = V_a - V_c = 56171.80 - 40520.12$ N $= 15651.68$ N. $A_{sv} = T_{sv}/f_{yv} =$

$15651.68/460 = 34.03$ mm^2. Provide $\phi 1.5 - 1 - 25 (= 33.93$ mm^2 within a distance $d = 240$ mm), as shown in Fig. 4a.

(ii) For excess tension due to bond failure (see Fig. A3) $\Delta z = (V_a - V_c) * X/(2T) = (56171.8 - 40520.12) * 33/(2 * 351859.2) \sim 1$ mm, $x' = 2(d - z - \Delta z) = 2(240 - 223.5 - 1) = 31$ mm, $\sigma_c' = C/(bx') = 351859.2/(200 * 31) = 56.8$ N/mm^2, $\sigma_{\text{conf}} = (\sigma_c' - \sigma_c)/5 = 0.64$ N/mm^2. Tensile stress resultant over a length of 100 mm $= 0.64 * 200 * 100 = 12800$ N. Required reinforcement is $A_{sv} = 12800/460 = 27.83$ mm^2. Use $\phi 1.5 - 2 - 25 (= 28.23$ mm^2 every 100 mm), as shown in Fig. 4a.

REFERENCES

1. BS 8110, *Structural use of concrete. Part 1. Code of practice for design and construction*, British Standard's Institution, London 1985.
2. ACI 318-89, *Building code requirements of reinforced concrete*, American Concrete Institute, Detroit 1989.
3. CAN 3-A23.3-M84, *Design of concrete structures for buildings*, Canadian Standards Association, Rexdale 1984.
4. CEB-FIP, *Model code for concrete structures*, Comité Euro-International du Beton, Cement and Concrete Association, London 1978.
5. W. RITTER, *Die Bauweise Hennebique*, Schweizerische Bauzeitung, **33**, 1899, 59–61.
6. E. MÖRSCH, *Concrete steel construction*, (English translation by E.P. Goodrich,) New York, McGraw-Hill, 1909, p. 368, (Translation from 3rd edition of Der Eisenbetonbau, 1st ed. 1902).
7. M.D. KOTSOVOS, I.D. LEFAS, *Behaviour of reinforced concrete beams designed in compliance with the concept of compressive force path*, ACI Struct. J., **87**, 2, 1990, 127–139.
8. M.D. KOTSOVOS, *Shear failure of reinforced concrete beams*, Engng Struct., **9**, 1, 1987, 32–38.
9. S.M. SERAJ, *Reinforced and prestressed concrete members designed in accordance to the compressive-force path concept and fundamental material properties*, Ph.D. Thesis, Imperial College, University of London, 1991.
10. M.P. COLLINS, *Towards a rational theory for RC members in shear*, J. Struct. Div., ASCE, **104**, 4, 1978, 649–666.
11. F.J. VECCHIO, M.P. COLLINS, *The modified compression-field theory for reinforced concrete elements subjected to shear*, ACI Struct. J., **83**, 2, 1986, 219–231.
12. J. SCHLAICH, K. SCHÄFER, M. JENNEWEIN, *Toward a consistent design of structural concrete*, Prestres. Concrete Institute J., **32**, 3, 1987, 74–150.
13. M.D. KOTSOVOS, *Compressive force path concept: basis for reinforced concrete ultimate limit design*, ACI Struct. J., **85**, 1, 1988, 68–75.
14. I.D. LEFAS, M.D. KOTSOVOS, N.N. AMBRASEYS, *Behaviour of reinforced concrete structural wall: strength, deformation characteristics and failure mechanisms*, ACI Struct. J., **87**, 1, 1990, 23–31.
15. A.H. ELZANATY, A.H. NILSON, F.O. SLATE, *Shear critical high strength concrete beams*, Research Report No. 85-1, Department of Structural Engineering, Cornell University, Ithaca 1985.

16. A.H. ELZANATY, A.H. NILSON, F.O. SLATE, *Shear capacity of reinforced concrete beams using high strength concrete*, ACI Struct. J., **83**, 2, 1986, 290–296.

17. A.G. MPHONDE, G.C. FRANTZ, *Shear strength of high strength concrete beams*, Report No. CE 84–157, Department of Civil Engineering, University of Connenticut, Storrs 1984.

18. A.G. MPHONDE, G.C. FRANTZ, *Shear tests of high and low strength concrete beams without stirrups*, ACI Struct. J., **81**, 4, 1984, 350–357.

19. F.K. KONG, R.H. EVANS, *Reinforced and prestressed concrete*, Van Nostrand Reinhold (International), 3rd edition, London 1987.

20. F. GONZALEZ VIDOSA, M.D. KOTSOVOS, M.N. PAVLOVIĆ, *Nonlinear finite-element analysis of concrete structures. Performance of a fully three-dimensional brittle model*, Comp. and Struct., **40**, 5, 1991, 1287–1305.

21. F. GONZALEZ VIDOSA, M.D. KOTSOVOS, M.N. PAVLOVIĆ, *A three-dimensional nonlinear finite-element model for structural concrete. Part 1. Main features and objectivity study*, Proc. ICE, Part 2, **91**, 4, 1991, 517–544.

22. F. GONZALEZ VIDOSA, M.D. KOTSOVOS, M.N. PAVLOVIĆ, *A three-dimensional nonlinear finite-element model for structural concrete. Part 2. Generality study*, Proc. ICE, Part 2, **91**, 4, 1991, 545–560.

23. S.M. SERAJ, M.D. KOTSOVOS, M.N. PAVLOVIĆ, *Three-dimensional finite-element modelling of normal- and high-strength reinforced concrete members, with special reference to T-beams*, Comp. and Struct., **44**, 4, 1992, 699–716.

BADANIE ŻELBETOWYCH BELEK Z BETONU O WYSOKIEJ WYTRZYMAŁOŚCI

Streszczenie

Praca stanowi część szerokiego programu badań, mającego na celu wprowadzenie jednolitego podejścia do projektowania konstrukcji żelbetowych i sprężonych z betonu o zwykłej lub wysokiej wytrzymałości. W obecnie stosowanych metodach projektowania elementów żelbetowych, *oparte na teorii wytrzymałości na zniszczenie*, stosowane są zasady niezgodne z podstawowym zachowaniem betonu jako materiału. W pracy wykazano na podstawie eksperymentalnej, że fizyczny model oparty na przebiegu drogi siły ściskającej, który uznawany jest jako przedstawiający w sposób racjonalny zachowanie elementów z betonu o zwykłej wytrzymałości, można również stosować do projektowania elementów z betonu o wysokiej wytrzymałości. Udowodniono ponadto, że osiągając graniczną wytrzymałość na zginanie, element nie zachowuje się zgodnie z teorią „kratownicową". Wręcz przeciwnie — projektowanie oparte na modelu kratownicy może być niewydajne i kosztowne. W pracy zamieszczono ograniczoną liczbę obliczeń parametrycznych i dodatkowych dowodów eksperymentalnych z poprzednich opracowań, które wykazują, że rola zbrojenia w półkach elementów z betonu o wysokiej wytrzymałości jest mniej widoczna niż w odpowiadających im elementach z betonu o zwykłej wytrzymałości. Zjawisko

to można wytłumaczyć różnym stopniem trójosiowości naprężeń występujących w elementach z betonu o zwykłej i wysokiej wytrzymałości.

BANGLADESH UNIVERSITY OF ENGINEERING
AND TECHNOLOGY, DHAKA, BANGLADESH,

NATIONAL TECHNICAL UNIVERSITY
OF ATHENS, GREECE

and

IMPERIAL COLLEGE OF SCIENCE, TECHNOLOGY
AND MEDICINE, UNIVERSITY OF LONDON, UK

Received January 17, 1994
Accepted May 4, 1994

Remarks on the paper should
be sent to the Editorial Board
not later than May 31, 1995